Morphology of Semicrystalline Block Copolymers of Ethylene-(Ethylene-*alt*-propylene)

Pratima Rangarajan and Richard A. Register*

Department of Chemical Engineering, Princeton University, Princeton, New Jersey 08544

Lewis J. Fetters

Exxon Research and Engineering Company, Annandale, New Jersey 08801

Received March 30, 1993; Revised Manuscript Received May 25, 1993

ABSTRACT: The morphology of a series of ethylene-(ethylene-*alt*-propylene) diblock copolymers (E/EP), in which microphase separation is driven by crystallization, has been investigated. The E/EP diblocks were prepared by catalytic hydrogenation of narrow-distribution butadiene-isoprene diblocks. All the diblocks crystallized from single-phase melts so that the morphology and domain size were not restricted by "freezing" of a microphase-separated melt. The E/EP diblocks adopted a lamellar morphology over the full range of compositions studied (E block fractions ranging from 0.12 to 0.56), and also exhibited spherulitic superstructure. Thus, unlike purely amorphous systems, the thicknesses of the E and EP domains are effectively decoupled and lamellar materials can be tailored with a wide range of compositions and domain thicknesses. The scaling of the lamellar spacing with molecular weight and composition is compared with theoretical predictions, and mild deviations are found. These may be due to the inability of a single stem of an E crystallite to span the entire E domain as the latter becomes progressively thicker. Evidence suggests that samples with thick E blocks contain multiple crystallites running parallel to the domain interfaces.

I. Introduction

Microphase separation and the resultant microdomain formation have been extensively studied in amorphous diblock copolymers. The threshold value of χN_t (where χ is the Flory interaction parameter and N_t is the total number of segments in the block copolymer) above which the system is heterogeneous is approximately 10.5 for a symmetric diblock copolymer.[1-3] Above this threshold value, phase diagrams have been developed that relate the microdomain morphology (such as spheres, cylinders, or lamellae) to the copolymer composition.[4,5] The analogous triblock copolymers, which have gained commercial popularity as thermoplastic elastomers (TPEs), also exhibit similar composition dependence in their microdomain morphologies. The glassy endblocks of these TPEs form physically-crosslinked microdomain structures within the rubbery matrix, thus imparting useful elastomeric properties. Well-organized microdomain structures require large block incompatibility (χN_t), but this often results in high-viscosity melts that make these materials difficult to process. Also, since the system is driven to minimize interfacial area, to a first approximation the morphology is given by the ratio of the lengths of the two blocks. This makes certain interesting morphologies impossible to obtain—for example, a lamellar structure where unlike lamellae are of greatly different thicknesses.

Microdomain formation in semicrystalline block copolymers can result either from incompatibility of the two blocks or by crystallization of one or both blocks. Prior experimental work by Cohen *et al.*[6] and Séguéla and Prud'homme[7] has demonstrated that the final morphology attained by semicrystalline block copolymers is path-dependent; different microdomain structures are obtained if microphase separation precedes crystallization or vice versa. Cohen *et al.*[6] studied the different morphologies attained by a styrene-ethylene (S/E) diblock (11 wt % E) when cast from solution at temperatures above and below the melting point (T_m) of the E block. When solvent is removed at temperatures above T_m, microphase separation occurs in the melt, and as the temperature is lowered, crystallization proceeds within the preexisting spherical microdomains of the E block. When solvent-casting is done below T_m, crystallization precedes microphase separation and there is no evidence of spherical microdomain morphology. Annealing below the T_m does not change the as-cast structure. Séguéla and Prud'homme[7] studied the difference in morphology and mechanical properties of ethylene-(ethylene-*alt*-propylene)-ethylene (E/EP/E) triblock copolymers when solvent-cast above and below the E block T_m. X-ray scattering data from the samples which were cast above the T_m show better microdomain ordering but lower crystallinity than the samples cast at room temperature. The mechanical properties of the melt-crystallized samples are similar to crosslinked elastomers whereas the solvent-cast samples behave like polyethylene of low crystallinity.

Nojima and co-workers[8] performed time-resolved SAXS on diblock copolymers of ϵ-caprolactone-butadiene (C/B) and studied the morphological changes as the copolymers are cooled from the melt to a temperature below both the T_m and the microphase separation temperature (T_s). In contrast to previous results, they find no morphological "freezing" of the microphase-separated morphology; the system cools from a homogeneous melt to a microphase-separated morphology which is destroyed by the subsequent crystallization. An important factor could be the proximity of the T_m to the T_s of the C/B diblock studied; crystallization occurs at a temperature just below the T_s, so that the energy barrier to disrupt the microdomain morphology is low and can be overcome by the subsequent crystallization.

Two models have been developed to describe the equilibrium morphology resulting from crystallization of one block of a diblock copolymer. Both models assume strict alternation of the amorphous and crystalline layers, an assumption supported by the tendency of crystallites to organize themselves in lamellae. An equilibrium degree of chain folding is proposed: a tradeoff between the fully-extended chain favored by the crystalline domain and the random coil configuration of amorphous chains. Mini-

* To whom correspondence should be addressed.

0024-9297/93/2226-4640$04.00/0

mization of free energy for the system results in a relationship between the interdomain spacing d, the number of statistical segments in the amorphous block N_a, and the total number of segments N_t. DiMarzio, Guttman, and Hoffman[9] (DGH) assumed equivalent segmental length for both blocks; further assuming equal density of the blocks leads to the scaling relation:

$$d \sim N_t N_a^{-1/3} \quad (1)$$

Whitmore and Noolandi (WN)[10] modeled the amorphous blocks as flexible chains described by a mean-field self-consistent theory, and the crystalline region as folded chains in a lamellar structure. The authors performed calculations using parameters specific to the styrene/ethylene oxide (S/EO) system to determine:

$$d \sim N_t N_a^{-5/12} \quad (2)$$

The scaling exponents derived by both theories are similar even though the S and EO segment lengths are very different. These relations can be compared with that for the lamellar structure formed in amorphous block copolymers,[4,11] for which $d \sim N_t^{2/3}$.

Since the theories are intended to describe the equilibrium morphology of semicrystalline block copolymers, experimental systems designed for comparison should possess sufficient mobility for equilibrium to be approached. In the C/B example, the driving force for crystallization is sufficiently large to promote a morphological rearrangement even in a microphase-separated sample. Douzinas *et al.*[12] used a series of diblock copolymers of ethylene–ethylethylene (E/EE) to experimentally evaluate the theoretically-predicted scaling laws, and found good agreement with eq 2. However, the processing history of the E/EE diblocks results in microphase separation prior to crystallization[13] which may produce the same sort morphological "freezing" as in the S/E case, where crystallization occurs within a preformed structure.

In this work, a series of diblock copolymers of ethylene–(ethylene-*alt*-propylene), E/EP, with crystallizable (E) block weight fractions (denoted f) ranging from 0.12 to 0.56 have been studied. Bates *et al.*[14] have determined χ for E/EP to be 0.007 at 120 °C, which is less than one-third that of E/EE, providing a substantial range of molecular weights and compositions over which the diblocks will form single-phase melts. Mechanical properties of E/EP diblocks and triblock analogues have previously been studied, but little information on the microdomain morphology has been presented.[7,15] The mechanical properties of the E/EP/E triblocks differ substantially from those of analogous polymers containing amorphous "hard" blocks, such as styrene–butadiene–styrene (SBS); for example, the E/EP/E systems[7] have higher moduli at low hard block content than the comparable SBS triblocks.[16] We thus investigate these diblocks to determine how their morphologies differ from those found in amorphous block copolymers and whether new structures may be obtained, as a model system to test the theoretical scaling relations, and as materials whose triblock analogues possess mechanical properties distinctly different from those of amorphous triblocks.

II. Experimental Section

A. Synthesis and Molecular Characterization. Precursor 1,4 isoprene–1,4 butadiene diblock copolymers were synthesized by sequential anionic polymerization in cyclohexane.[17] The E/EP diblocks were prepared from the precursors by exhaustive hydrogenation at 80 °C and 400 psi in heptane using unpoisoned palladium on calcium carbonate (or barium sulfate) as catalyst.[18]

Table I. E/EP Molecular Characterization Data

sample	M_w (kg/mol)	f	ethyl branches/1000 C
15/111	126	0.12	22
8/46	54.3	0.15	18
11/44	54.6	0.21	18
30/87	117	0.26	24
19/30	48.8	0.38	14
5/8	13.4	0.41	18
11/14	25.3	0.44	26
11/8	18.9	0.56	18

^{1}H nuclear magnetic resonance (NMR) of the available precursors was used to determine the weight fraction of butadiene block (f, ±3%/total E block), the percent 3,4 addition in the isoprene (5–8%) and the percent 1,2-addition in the butadiene block. Due to the unavailability of the precursors for samples 15/111, 5/8, and 11/14, high-temperature (80 °C) ^{13}C-NMR was used, instead of ^{1}H-NMR, to characterize the hydrogenated diblocks. Fourier transform infrared spectroscopy (FTIR) was used to verify that the samples had undetectable residual unsaturation (<1 double bond/100 carbons). Molecular weights and polydispersities of the precursor diblocks were determined by low-angle laser light scattering (LALLS; Chromatix KMX-6) in cyclohexane and by gel permeation chromatography (GPC; Waters, in tetrahydrofuran). Since the refractive index increments (dn/dc) of the butadiene and isoprene blocks are very similar in cyclohexane, the LALLS data were analyzed using a single dn/dc value[19] of 0.105 cm^3/g. High-temperature sequential GPC/LALLS of the E/EP diblocks, at 135 °C in trichlorobenzene, showed that no backbone changes occurred as a result of hydrogenation. The molecular characterization results are listed in Table I. The diblocks are identified by the following sample code: $M_{w(E)}$ (kg/mol)/$M_{w(EP)}$ (kg/mol). The 1,2-additions in the butadiene block, upon hydrogenation, become pendant ethyl branches on the E chains; the percent 1,2-addition has been used to calculate the ethyl branches per 1000 backbone carbons in the E block of each sample, also reported in Table I. A similar density of isopropyl branches is produced in the EP block by hydrogenation of the 3,4-isoprene units.

B. Morphological Characterization. The E/EP diblocks were heated to 124 °C in polytetrafluoroethylene dishes under either vacuum or nitrogen and allowed to flow under their own weight into films. The temperature was then slowly lowered (~20 °C/h) to 70–84 °C, and the samples were allowed to anneal for a minimum of 24 h. Densities were determined with an ethylene glycol–methanol column held at 23 °C and calibrated from 0.8492 to 0.9095 g/cm^3 (±0.0002). A Perkin-Elmer DSC-4 run at 20 °C/min was used to determine the final melting temperature (T_m) and the enthalpy of melting (ΔH_m) after baseline subtraction. DSC calibration was performed using an indium standard. Wide-angle X-ray scattering (WAXS) data, in reflection mode, were collected on a Phillips-Norelco wide range goniometer with a graphite crystal focusing monochromator. Small-angle X-ray scattering (SAXS), using a compact Kratky camera and a Braun position sensitive detector, was used to probe the room-temperature morphology of the samples. Data were collected and reduced using previously reported procedures[20] and expressed as the background-subtracted, desmeared absolute intensity I/I_eV versus the scattering vector $q = (4\pi/\lambda)\sin\theta$; I_e is the scattering from a single electron, V is the illuminated scattering volume, λ is the radiation wavelength, and 2θ is the scattering angle. The background was found to be well-described by the form $(A + Bq^4)$, where B was held constant at 0.070 nm and A varied between samples. Small-angle light scattering (SALS) H_v patterns were obtained with a helium–neon laser using the photographic technique developed by Stein.[21] The results of morphological characterization are summarized in Table II.

III. Results and Discussion

Molecular weights of the diblocks ranged from 13 to 126 kg/mol, with f ranging from 0.12 to 0.56, providing an adequate range of composition to study the scaling relations. All the samples except for 30/87 were free from low molecular weight products of early termination, as shown by GPC, and had polydispersities less than 1.07.

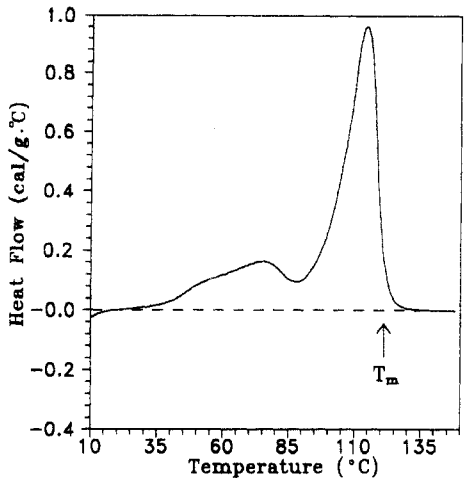

Figure 1. DSC data for sample 11/8. Dashed line indicates the baseline; the arrow indicates the position of final melting temperature T_m.

Table II. E/EP Morphological Characterization Data

sample	q^* (nm^{-1})	ρ (g/cm^3)	d (nm)	final T_m (°C)	w_c^c (DSC)	w_c^d (density)	w_c^x (WAXS)
15/111	0.102	0.8624	61.6	119	0.49	0.61	0.40
8/46	0.118	0.8653	53.2	112	0.54	0.65	0.40
11/44	0.115	0.8693	54.6	120	0.56	0.62	0.42
30/87	0.110	0.8700	57.1	107	0.36	0.52	0.30
19/30	0.113	0.8825	55.6	123	0.56	0.63	0.43
5/8	0.214	0.8846	29.4	114	0.58	0.62	0.47
11/14	0.171	0.8848	36.7	109	0.38	0.58	0.33
11/8	0.192	0.8933	32.7	123	0.57	0.58	0.42

Sample 30/87 has a long tail which is suspected to be low molecular weight diblock, resulting in a polydispersity of 1.21. Although the morphology of sample 30/87 will be discussed, it will not be used to test the scaling relations.

A small percentage of vinyl substitution in the precursor butadiene block results, upon hydrogenation, in pendant ethyl branches on the polyethylene chain. Only about 10% of the ethyl branches are incorporated into the crystallites.[22] The polyethylene chain is, therefore, forced to exit a crystallite when it encounters an ethyl branch. This should restrict the size and the ordering of the crystallites. Most of the samples had 14–18 (±3) ethyl branches/1000 backbone carbons in the E block, although samples 15/111, 30/87, and 11/14 registered values between 22 and 26.

The final T_m values for the diblocks were determined as the baseline intercept of the tangent to the downward slope of the melting endotherm (Figure 1). All the samples show T_m values comparable to literature values for similar hydrogenated polybutadienes.[23,24] A hydrogenated polybutadiene of similar ethyl branch content studied in this laboratory displayed a T_m of 115 °C. Although the shape of the melting curve, particularly the low-temperature end, could be manipulated somewhat through the annealing temperature, the annealing regimen had no perceptible effect on the total heat of fusion (ΔH_m) or on the SAXS patterns. To quantify the extent of crystallinity in each sample, normalized to the content of E block, a weight fraction crystallinity w_c^c was calculated from ΔH_m by:

$$w_c^c = \frac{\Delta H_m}{(\Delta H_{m,PE})f} \tag{3}$$

$\Delta H_{m,PE}$ is the theoretical heat of fusion for 100% crystalline polyethylene (66.2 cal/g).[25] The WAXS data were also used to determine an analogous quantity, w_c^x:

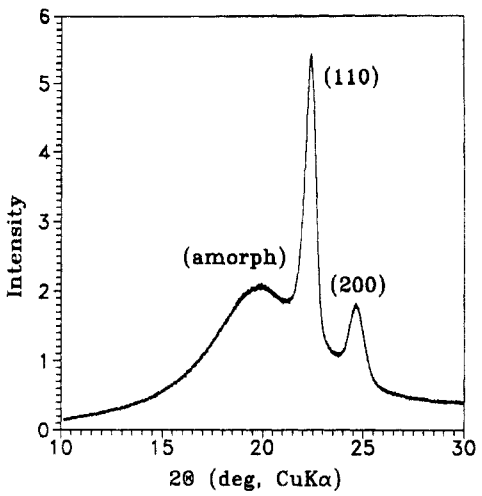

Figure 2. WAXS data for sample 11/8. The (110) and (200) crystalline polyethylene peaks are riding on a broad amorphous halo (amorph).

$$\frac{\text{area}[(110)+(200)]}{\text{area (amorphous)}} = \frac{w_c^x f}{1 - w_c^x f} \tag{4}$$

As shown in Figure 2, the (110) and (200) reflections of polyethylene are clearly visible, riding on a broad amorphous halo contributed by both the EP block and amorphous E regions. A third measure of the weight fraction crystallinity was determined from the copolymer densities:

$$\frac{1}{\rho} = \frac{1-f}{\rho_{EP}} + \frac{f(1-w_c^d)}{\rho_{E,a}} + \frac{w_c^d f}{\rho_{E,c}} \tag{5}$$

ρ, ρ_{EP}, $\rho_{E,a}$, and $\rho_{E,c}$ are the densities of the copolymer, the EP material, the amorphous fraction of the E block, and the E crystallites respectively. ρ_{EP}[14,26] is taken to be 0.8539 g/cm^3 at 23 °C; $\rho_{E,c}$ is taken to be 0.986 g/cm^3 based on the unit cell dimensions of similar hydrogenated polybutadienes.[23] By extrapolation of density data (23 °C) for amorphous hydrogenated polybutadienes with varying ethyl branch content,[26] $\rho_{E,a}$ is estimated at 0.856 g/cm^3 for a hydrogenated polybutadiene containing 20 ethyl branches per 1000 backbone carbons. Crystallinity values by DSC were consistently 1.3 times the values found by WAXS, while those found from density measurements averaged 1.5 times those from WAXS, since interfacial material and poorly-ordered crystallites are likely to be counted as amorphous material in the WAXS data. These crystallites contribute to both the density and the melting enthalpy, appearing as a broad, low-melting hump in the DSC data of Figure 1. T_m, w_c^c, and w_c^x values for samples 30/87 and 11/14 are much lower than the other samples, due to the large number of ethyl branches in the E blocks of these samples. Sample 15/111 does not show similarly-low values for T_m and w_c, despite a similar ethyl branch content from ^{13}C NMR; however, the ethyl branch resonances are weak in this sample because of its low E block content (12%), so the branch content reported in Table I is correspondingly more uncertain. The w_c values determined by density seem less sensitive to variations in the ethyl branch content than w_c values from DSC or WAXS.

The degree of interdomain ordering can be determined by SAXS, as shown in Figure 3. Since the theoretically-predicted morphology is lamellar, the ordinate is multiplied by q^2, to account for the angular dependence of the form factor scattering from lamellae. The Bragg spacing (equivalent to the repeat distance d for a lamellar

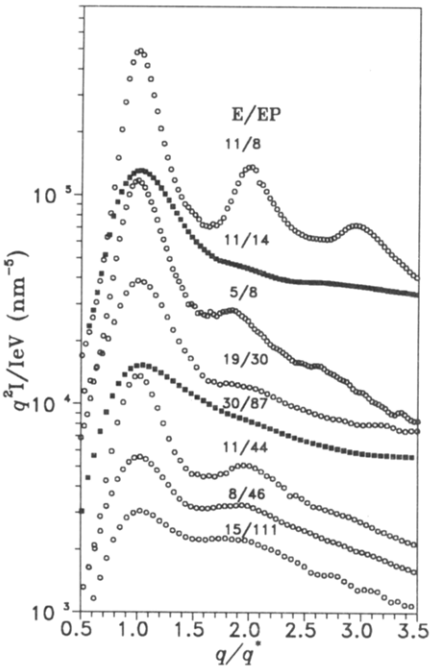

Figure 3. SAXS data for the E/EP diblocks. The abscissa is scaled by the position of the principal reflection q^*. Key: (○) well-ordered samples (at least 2 peaks at q/q^* of 1:2); (■) poorly ordered samples (large ethyl branch content in E block). The intensities have been scaled by the following factors for clarity: 11/8, 15; 11/14, 13.3; 5/8; 19/30, 1.5; 30/87, 2.2; 11/44, 0.8; 8/46, 0.8; 15/111, 0.6.

morphology) is calculated from the position q^* of the first SAXS peak in a plot of q^2I vs q:

$$d = \frac{2\pi}{q^*} \tag{6}$$

q^* is reproducible with an accuracy better than ±1% for all but samples 15/111 and 19/30, where the peak occurs close to the beamstop and reproducibility drops to ±3%. Since a lamellar morphology will result in higher-order peaks appearing at q values which are integral multiples of q^*, the abscissa has been normalized by q^* in Figure 3. SAXS data for sample 11/8 show peaks at q/q^* ratios of 1:2:3, indicating the presence of a well-ordered lamellar morphology. This copolymer has a near-symmetric composition (f = 0.56) and should form lamellae even in a purely amorphous diblock. However, there is at most a hint of a second peak in the SAXS data for samples 30/87 and 11/14. The lack of ordering in these samples correlates with their low T_m and w_c values; all can be attributed to the samples' large ethyl branch contents. The relationship between the degree of ordering and the E block crystallinity is consistent with crystallization-driven microdomain formation; if microphase separation were driven by block incompatibility, the degree of ordering would improve with increasing χN_t so sample 30/87, which has large N_t, should be well-ordered. Sample 5/8 has a very low molecular weight, which results in small domain widths and relatively thick interfaces. The diffuse interfaces in turn produce a steep downward slope in the SAXS data, causing the second-order peak to appear at slightly less than $2q^*$. The remaining samples all show two peaks in a 1:2 ratio, to within experimental error, indicating a lamellar structure. Samples 15/111 and 8/46 have very asymmetric compositions which would lead to spherical domains in a purely amorphous copolymer (SAXS peaks at q/q^* of 1:$\sqrt{2}$:$\sqrt{3}$). Thus the assumption underlying the theoretical treatments—that a lamellar morphology is adopted even for very asymmetric compositions—appears valid even for f = 0.12.

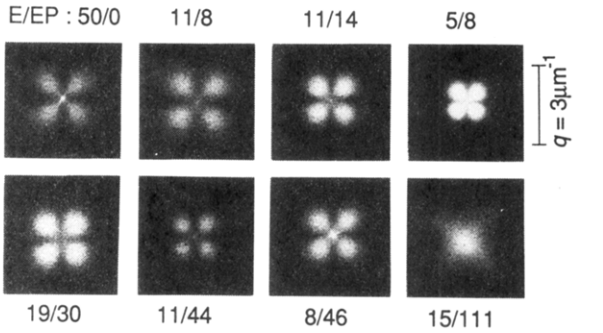

Figure 4. H_v SALS patterns for a hydrogenated polybutadiene (50/0) and selected E/EP samples. Spherulitic superstructure is observed down to f = 0.12 (sample 15/111).

Further evidence of lamellar microdomain morphology is provided by the presence of spherulites, which are formed by radial growth of crystalline lamellae. H_v SALS photographs for some of the samples are reproduced in Figure 4. The four-leaf-clover pattern, the signature of spherulitic superstructure, was obtained for the full range of compositions studied here. The spherulite radius R_s is determined from[21]:

$$R_s = \frac{4.1}{q\dagger} \tag{7}$$

where $q\dagger = (4\pi/\lambda) \sin\theta$ at the position of maximum intensity. The only sample which does not show the cloverleaf pattern in H_v SALS is 30/87; this may be due to its high concentration of ethyl branches and a substantial variation in E content between chains, due to the low molecular weight tail. The spherulite radii ranged from 4 to 8 μm, values between those reported for E/EP/E triblocks[27] and linear low-density polyethylene.[28] A hydrogenated polybutadiene (designated 50/0 in Figure 4) of microstructure similar to the E blocks showed a spherulite radius of ~5 μm.

The overwhelming evidence that these semicrystalline diblocks form an alternating lamellar morphology at all compositions is contrary to the conclusions of other groups who have worked on E/EP/E triblocks. Mohajer *et al.*[15] found that the initial modulus of a symmetric E/EP/E triblock (50% E) is similar to that of an SBS triblock[16] containing 40% S. In contrast, the moduli reported for the 18 and 27% E block samples are much greater than the modulus of SBS with 28% S. This implies that the 18% and 27% E block samples have more continuous "hard" domains than an SBS triblock with a cylindrical morphology. It is also very interesting to note that the 7% E block sample shows a modulus comparable to the 28% S block SBS. Spherulitic superstructure was also observed in the E/EP/E triblocks[15] down to 27% E block. The authors concluded that the low E block samples formed spherical E domains which act as tethers to prevent slippage of the midblock chains. Séguéla and Prud'homme[7] investigated a similar 27% E triblock and concluded that the melt-crystallized sample formed a cylindrical microdomain structure as it would in a purely amorphous system.

As discussed in the Introduction, the solid-state morphology of crystallizable block copolymers may be substantially influenced by the structure of the melt. The first experimental indication that the E/EP diblocks used in this study form single-phase melts was that the samples flowed under their own weight[29] at 124 °C. $\chi N_t'$ for each diblock was calculated using[14] χ = 0.007 (at 397 K) and plotted on a reproduction of Leibler's[1] phase diagram (Figure 5). As in ref 14, $N_t' = M_n/m_o$, where M_n is the number-average molecular weight and m_o is the mer

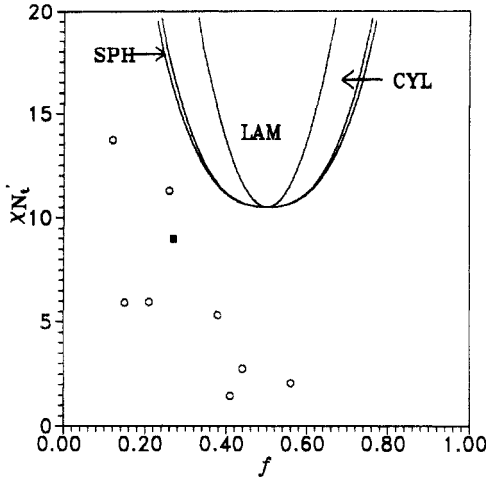

Figure 5. $\chi N_t'$ (124 °C) vs f data plotted on Leibler's phase diagram. Reproduced with permission from ref 1. Copyright 1980 American Chemical Society. Key (○) E/EP data (this work); (■) Séguéla and Prud'homme E/EP/E sample.

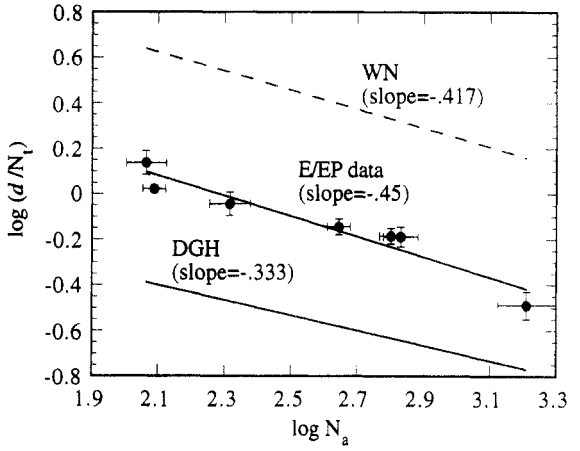

Figure 6. Scaling plot with experimental data and theoretical predictions. Error bars denote confidence intervals (errors in N_t, f, and d). The theoretical curves have been offset for clarity.

molecular weight (taken to be 60 for both blocks). The $\chi N_t'$ value for each sample falls well below that at the microphase separation transition (MST) indicating that the samples should indeed form single-phase melts. A single-phase melt is consistent with the lamellar microdomain morphology adopted by samples 15/111 and 8/46; if these samples had formed heterogeneous melts the spherical melt morphology would probably have been frozen in, as their high molecular weights would have hindered chain mobility and rearrangement. A calculation of $\chi N_t'$ (using the triblock $N_t'/2$) for the Séguéla and Prud'homme[7] copolymer yields a value of ~9, which also falls in the single-phase region of Figure 5.

Since microphase separation is driven by crystallization from a single-phase melt in our E/EP polymers, the thicknesses of the E and EP domains are effectively decoupled; the unlike lamellae do not have to be of comparable thickness for the morphology to be thermodynamically stable. Also, since the E/EP materials crystallize from a single-phase melt, they should be able to more nearly approach the equilibrium morphology, and thus may represent a valid system for comparison with the theoretical domain scaling laws. Figure 6 shows the experimental data and theoretical scaling laws (offset from the data for clarity) on a plot of log (d/N_t) vs. log (N_a), where the N values are calculated based on the weight-average number of butadiene or isoprene units in the precursor diblocks. The DGH, WN, and experimental scaling exponents are −0.333, −0.417 and −0.45 (±0.07 standard deviation), respectively. Although the statistical

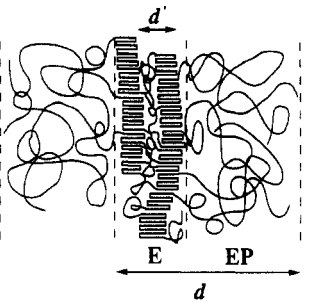

Figure 7. Proposed morphology for E/EP diblock copolymers crystallized from a single-phase melt. d is the total lamellar repeat distance: sum of the E and EP domain widths. d' is the repeat distance within the E domain: sum of the E crystallite thickness and amorphous E regions.

segment lengths of the E and EP blocks are quite similar at any temperature (R_g^2/N values of 11.6 and 9.6 Å^2 respectively[30-33] at 140 °C, and $d(\ln R_g^2)/dT \approx -0.0011$ K^{-1} for both[31,33]), the scaling exponent is quite different from the DGH exponent and is closer to the WN value.

It should be noted that the scatter of the data in Figure 6 about the best-fit line is a little larger than warranted by experimental error, as indicated by the bars representing the confidence limits. Defining the N values based on M/m_o, as for the phase diagram in Figure 5, produces a best-fit slope of −0.48, with similar scatter. Samples 8/46 and 11/44, which have very similar values of N_a and N_t, are in close proximity on the scaling plot, which lends confidence to the accuracy of the experimental measurements. However, samples 5/8 and 11/8, which have very similar values of N_a but differing values of N_t, are rather far apart on the plot, and the best-fit line does not pass close to either point. This suggests that the theories do not provide a completely accurate description of the effect of the crystalline block on the domain spacing in these E/EP diblocks. One explanation may be that the system studied here does not conform exactly to the theories, which assume that a crystalline stem can span the entire crystalline block domain and that an equilibrium level of chain folding, which is reflected in the scaling laws, is induced solely by the attachment of the amorphous block. In our materials, the presence of ethyl branches in the E block can also prevent an E crystallite from spanning the entire E domain, for sufficiently long E blocks, and thus influence the domain thickness.

In all these materials, the degree of crystallinity of the E block is substantially less than 100%, which raises the question: where is the amorphous E material? One possibility is that the E domains have the thickness of a single crystallite (governed by the number of ethyl branches), and that the amorphous E material is all at the domain interfaces or mixed with the EP block. A more likely possibility, particularly when the E blocks are long, is that the E domain resembles a semicrystalline homopolymer, with alternating crystalline and amorphous layers. This situation is shown schematically in Figure 7. As the E block becomes longer, the E domain becomes thick enough to accomodate multiple crystallites running parallel to the domain interfaces. In this case, as the E domain thickens, SAXS should show a buildup of intensity at a q value corresponding to the intercrystallite repeat, as seen in the hydrogenated polybutadiene 50/0 ($q \sim 0.48$ nm^{-1}; $d' = 13$ nm). Inspection of the SAXS profiles reveals that there is, indeed, a broad hump centered at $q \sim 0.5$ nm^{-1} in the data for samples 30/87, 19/30, and 11/14 (Figure 8). These humps can be compared with the profile for sample 11/44, which is featureless in this region, and with the data for the hydrogenated polybutadiene homopolymer (50/0). Samples 30/87, 19/30, and 11/14 are three of the

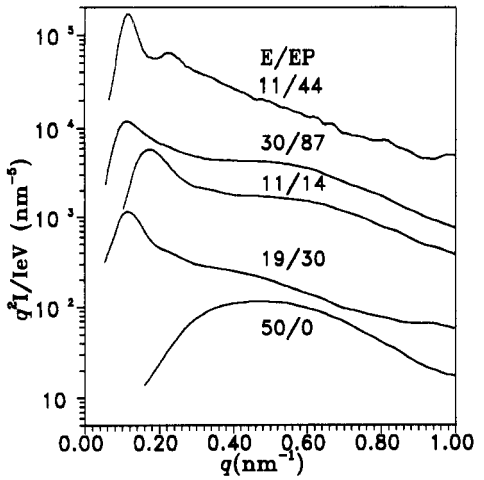

Figure 8. SAXS data for four E/EP diblocks and a hydrogenated polybutadiene (50/0). Note hump present in bottom four data sets near $q^* \sim 0.5$ nm^{-1}. The data sets have been scaled by the following factors for clarity: 11/44, 10; 30/87, 1.7; 11/14, 0.6 ; 19/30, 0.05; 50/0, 0.01.

four samples that have overall E domain widths ($d_E = v_f d$ where v_f is the volume fraction of E) calculated to be larger than d'. The fourth sample (11/8) does not show this hump because the higher-order reflections due to microphase separation of E and EP obscure any other features in this angular region. These results suggest that when d_E is large, the E domain resembles that of the hydrogenated polybutadiene homopolymer.

IV. Conclusions

The microdomain morphology of a series of semicrystalline E/EP diblock copolymers has been investigated. On the basis of literature values of χ, all materials are expected to possess a single-phase melt, so that microdomain formation should be crystallization-driven. SAXS data for all but two of the samples showed at least two peaks at integral multiples of q^* indicating the presence of alternating lamellar microdomains. For samples in which the E block contains a large density of ethyl branches, poor microdomain ordering was obtained, as evidenced by a single SAXS peak, further supporting the idea that crystallization drives microphase separation in these materials. Further evidence of lamellar morphology was the observation of the four-leaf-clover pattern in H_v SALS, the signature of spherulitic superstructure, for the full range of compositions studied here (down to $f = 0.12$). Thus, in the E/EP system, the thicknesses of the E and EP domains are decoupled and lamellar materials can be tailored with a wide range of hard block fractions and domain widths.

The presence of lamellar microdomains at all compositions validates theoretical assumptions, and this system can, therefore, be used to test the domain scaling relationships. The lamellar domain spacing d is found to scale roughly as $d \sim N_t N_a^{-0.45}$, although the scaling exponent of −0.45 is found to be greater in magnitude than both the DGH and the WN theoretical predictions. Furthermore, this simple scaling does not reproduce the d values to within experimental error. This discrepancy could result from the presence of ethyl branches in the E block which prevent a crystalline E stem from spanning the entire E domain, a factor not considered in the theoretical treatments. Three samples with relatively long E blocks show a broad peak at $q^* \sim 0.5$ nm^{-1}, reminiscent of the scattering seen in hydrogenated polybutadiene, suggesting that thick E domains contain multiple crystallites running parallel to the domain interfaces.

Acknowledgment. Acknowledgment is made to the donors of the Petroleum Research Fund, administered by the American Chemical Society, and to the National Science Foundation, Polymers Program (Grants DMR-9121294 and DMR-9257565) for partial support of this research. Fellowship support for P.R. was generously provided by General Electric, Chevron, Procter & Gamble, and the Shell Foundation. We thank Dr. Gary Ver Strate of EXXON Chemical Co. for the high temperature GPC/LALLS data, and Ramanan Krishnamoorti of Princeton University for help with the hydrogenation.

References and Notes

(1) Leibler, L. *Macromolecules* **1980**, *13*, 1602.
(2) Frederickson, G. H.; Helfand, E. *J. Chem. Phys.* **1987**, *87*, 697.
(3) Bates, F. S.; Bair, H. E.; Hartney, M. A. *Macromolecules* **1984**, *17*, 1987.
(4) Helfand, E.; Wasserman, Z. R. In *Developments in Block Copolymers—1*; Goodman, I., Ed.; Applied Science: New York 1982.
(5) Molau, G. E. In *Block Copolymers*; Aggarwal, S. L., Ed.; Plenum: New York, 1970.
(6) Cohen, R. E.; Cheng, P. L.; Douzinas, K.; Kofinas, P.; Berney, C. V. *Macromolecules* **1990**, *23*, 324.
(7) Séguéla, R.; Prud'homme, J. *Polymer* **1989**, *30*, 1446.
(8) Nojima, S.; Kato, K.; Yamamoto, S.; Ashida, T. *Macromolecules* **1992**, *25*, 2237.
(9) DiMarzio, E. A.; Guttman, C. M.; Hoffman, J. D. *Macromolecules*, *13*, 1194.
(10) Whitmore, M. D.; Noolandi, J. *Macromolecules* **1988**, *21*, 1482.
(11) Hashimoto, T.; Shibayama, M.; Kawai, H. *Macromolecules* **1980**, *13*, 1237.
(12) Douzinas, K. C.; Cohen, R. E.; Halasa, A. F. *Macromolecules* **1991**, *24*, 4457.
(13) Douzinas, K. C.; Cohen, R. E. *Macromolecules* **1992**, *25*, 5030.
(14) Bates, F. S.; Schulz, M. F.; Rosedale, J. H.; Almdal, K. *Macromolecules* **1992**, *25*, 5547.
(15) Mohajer, Y.; Wilkes, G. L.; Wang, I. C.; McGrath, J. E. In *Elastomers and Rubber Elasticity*: Mark, J. E.; Lal, J. Eds.; ACS Symposium Series 193; American Chemical Society: Washington, DC, 1982.
(16) Holden, G.; Bishop, E. T.; Legge, N. R. *J. Polym. Sci. C* **1969**, *26*, 37.
(17) Morton, M.; Fetters, L. J. *Rubber Chem. Technol.* **1975**, *48*, 359.
(18) Rosedale, J. H.; Bates, F. S. *J. Am. Chem. Soc.* **1988**, *110*, 3542.
(19) Hadjichristidis, N.; Xu, Z.; Fetters, L. J.; Roovers, J. *J. Poly. Sci., Polym. Phys. Ed.* **1982**, *20*, 743.
(20) Register, R. A.; Bell, T. R. *J. Polym. Sci. B: Polym. Phys.* **1992**, *30*, 569.
(21) Stein, R. S. *Rubber Chem. Technol.* **1976**, *49*, 458.
(22) Hosoda, S.; Nomura, H.; Gotoh, Y.; Kihara, H. *Polymer* **1990**, *31*, 1991.
(23) Howard, P. R.; Crist, B. *J. Polym. Sci. B: Polym. Phys.* **1989**, *27*, 2269.
(24) Krigas, T. M.; Carella, J. M.; Struglinski, M. J.; Crist, B.; Graessley, W. W. *J. Polym. Sci. B: Polym. Phys.* **1985**, *23*, 509.
(25) Brandrup, J., Immergut, E. H. Eds., *Polymer Handbook*, 3rd ed.; Wiley: New York, 1989.
(26) Krishnamoorti, R.; Balsara, N. P.; Lohse, D. J.; Fetters, L. J.; Schulz, D. N.; Sissano, J. A.; Graessley, W. W. To be published.
(27) Mohajer, Y.; Wilkes, G. L.; Wang, I. C.; McGrath, J. E. *Polymer* **1982**, *23*, 1523.
(28) Hu, S.-R.; Kyu, T.; Stein, R. S. *J. Polym. Sci. B: Polym. Phys.* **1987**, *25*, 71.
(29) Bates, F. S.; Rosedale, J. H.; Bair, H. E.; Russell, T. P. *Macromolecules* **1989**, *22*, 2557.
(30) Horton, J. C.; Squires, G. L.; Boothroyd, A. T.; Fetters, L. J.; Rennie, A. R.; Glinka, C. J.; Robinson, R. A. *Macromolecules* **1989**, *22*, 681.
(31) Boothroyd, A. T., Rennie, A. R.; Boothroyd, C. B. *Europhys. Lett.* **1991**, *15*, 715.
(32) Hattam, P.; Gauntlett, S.; Mays, J. W.; Hadjichristidis, N.; Young, R. N.; Fetters, L. J. *Macromolecules* **1991**, *24*, 6199.
(33) Zirkel, A.; Richter, D.; Pyckhout-Hintzen, W.; Fetters, L. J. *Macromolecules* **1992**, *25*, 954.